THE JOURNAL OF PHYSICAL CHEMISTRY B

ARTICLE

pubs.acs.org/JPCB

New Monte Carlo Simulation of Adsorption of Gases on Surfaces and in Pores: A Concept of Multibins

Chunyan Fan, D. D. Do,* and D. Nicholson

School of Chemical Engineering, University of Queensland, St. Lucia, Qld 4072, Australia

ABSTRACT: We introduce a new and effective Monte Carlo scheme to simulate adsorption on surfaces and in pores. The simulation box is divided into bins to account for the nonuniform distribution of particle density, and the new scheme takes into account the state of each bin and allows the maximum displacement length to vary with the bin density. The probability of acceptance of insertion and deletion from a bin depends on the density of the fluid in that bin, rather than on the average density in the whole simulation box. In other words, our scheme is local. We apply this new scheme to a canonical ensemble and a grand canonical ensemble, and because it is based on exchange of particles between bins of different density, we refer to this new method as Multibin Canonical Monte Carlo (*Mu*-CMC) and Multibin Grand Canonical Monte Carlo (*Mu*-GCMC). The process of particle exchange within the canonical ensemble makes the new scheme much more efficient, compared to conventional canonical ensemble simulation. We apply the new scheme to a number of adsorption systems to illustrate its potential.

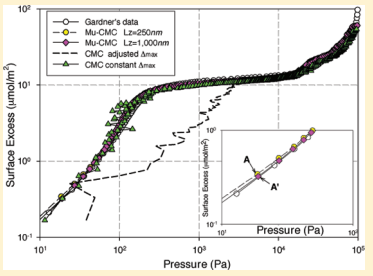

1. INTRODUCTION

Monte Carlo (MC) and Molecular Dynamics (MD) simulations have been extensively used with success to study adsorption systems during the last few decades.[1−11] These systems are inherently nonuniform, although the question of nonuniformity in the density is rarely discussed in the literature.

A typical problem is that the theory of Monte Carlo does not give us any information about the choice of the MC parameters and how it is implemented. As long as microscopic reversibility is adhered to, equilibrium will be eventually achieved. Often, practitioners choose the MC parameters and the implementation, based on experience or from some ad hoc premise such as the collection of a "control chart" during the simulation. Mountain and Thirumalai[12] made a detailed study of efficiency in Monte Carlo simulation and suggested an acceptance ratio of 0.2 as the optimal criterion for a displacement move. Their test was applied to a Lennard-Jones liquid near the triple point (at a reduced density, $\sigma^3\rho$ of 0.85, and a reduced temperature of 0.88), but their study is restricted to a homogeneous fluid, in which each particle is isotropically surrounded by the same number of neighbors. In adsorption systems, however, the confined fluid is strongly nonuniform, especially when its state is close to a phase separation, and different schemes are needed to deal with the variation of the adsorption density. To highlight this statement, consider a problem that can occur in GCMC: Creation and destruction moves in these simulations use an acceptance/rejection criterion that depends on the number of particles currently in the system. In a uniform fluid, this causes no difficulties, but in nonuniform systems the number can vary in space. For the relatively small systems usually studied, this does not present a problem, but in very large systems, as we demonstrate below, a local particle density needs to be considered.

In this paper, we propose a new and effective scheme to study the equilibrium of adsorption systems. We introduce the concept of using separate bins such that each bin is approximately the same with respect to the interaction energy between particles. We apply this to both canonical ensemble and grand canonical simulations and coin the term Multibin Canonical Monte Carlo (*Mu*-CMC) simulation and Multibin Grand Canonical Monte Carlo (*Mu*-GCMC) for the new scheme. A number of adsorption systems are used to illustrate the potential of our new Monte Carlo schemes.

2. THEORY

To simulate the adsorption isotherm and isosteric heat, we use either the Canonical ensemble or the Grand Canonical ensemble in the Monte Carlo (MC) simulation, details of which can be found in ref 13, and here we summarize the main points used in our simulations. To simulate adsorption on a graphite surface, we use a rectangular simulation box, the bottom of which is the graphite surface, while the top is modeled as a hard wall. This does not seriously perturb the system for the subcritical adsorption systems studied in this paper.[14]

2.1. Fluid−Fluid Potential. Argon is modeled as a single LJ site. The interaction energy between particle "*i*" with particle "*j*" is described by the Lennard-Jones 12-6 equation

$$\phi_{i,j} = 4\varepsilon\left[\left(\frac{\sigma}{r_{i,j}}\right)^{12} - \left(\frac{\sigma}{r_{i,j}}\right)^{6}\right] \quad (1)$$

Received: June 12, 2011
Revised: July 19, 2011
Published: July 29, 2011

where $r_{i,j}$ is the distance between the centers of particles i and j. For molecular parameters for argon, we choose values that reproduce the vapor−liquid equilibrium and adsorption on graphite well:[15] collision diameter σ = 0.3405 nm, reduced well depth ε/k_B = 119.8 K.

2.2. Solid−Fluid Potential. The solid−fluid interaction energy between a particle i and the homogeneous flat solid substrate is calculated by the following 10−4−3 Steele potential[16,17]

$$\phi_{i,s} = 2\pi\rho_s\varepsilon_{sf}\sigma_{sf}^2\left\{\frac{2}{5}\left(\frac{\sigma_{sf}}{z_i}\right)^{10} - \left(\frac{\sigma_{sf}}{z_i}\right)^{4} - \frac{\sigma_{sf}^4}{3\Delta(0.61\Delta + z_i)^3}\right\} \quad (2)$$

where ρ_s is the surface carbon atom density of a graphene layer (38.2 nm^{-2}) and Δ is the spacing between the two adjacent graphite layers (0.3354 nm). The solid−fluid molecular parameters, the collision diameter σ_{sf}, and the interaction energy ε_{sf} are calculated from a modified Lorentz−Berthelot mixing rule in which the interaction parameter is adjusted by the introduction of a binary interaction parameter, k_{sf}, such that the experimental Henry constant is reproduced by the GCMC simulations, that is $\varepsilon_{sf} = (1 - k_{sf})(\varepsilon_{ff}\varepsilon_{ss})^{1/2}$. For simplicity we assume that the binary interaction parameter, k_{sf}, is the same for all interaction sites of a molecule. In this study, for argon adsorption on a graphitized surface, we choose k_{sf} = 0.015, which is obtained by matching the simulation results with the experimental data at 87.3 K.

2.3. Monte Carlo Scheme. In this work, we introduce Multibin Canonical ensemble and Multibin Grand Canonical ensemble Monte Carlo simulations to determine the adsorption isotherm and isosteric heat. The parameters used in the simulation are: (i) the cutoff radius which is set to half of the xy box length along which directions the periodic boundary conditions are applied or five times the collision diameter, whichever is smaller, and (ii) the number of cycles for the equilibration and sampling stages: 50 000 for conventional CMC or GCMC, while in *Mu*-CMC and *Mu*-GCMC it depends on the number of bins and is chosen such that the total number of configurations is equal to that in the conventional CMC and GCMC.

2.3.1. Multibin Grand Canonical Monte Carlo. The probabilities for acceptance for the three moves in standard GCMC are:[13]

1. Displacement:

$$p = \min\{1, \exp(-\Delta U/kT)\} \quad (3a)$$

2. Insertion:

$$p = \min\left\{1, \frac{V}{\Lambda^3(N+1)}\exp\left[\frac{\mu - U(N+1) + U(N)}{kT}\right]\right\} \quad (3b)$$

3. Deletion:

$$p = \min\left\{1, \frac{\Lambda^3 N}{V}\exp\left[-\frac{\mu + U(N-1) - U(N)}{kT}\right]\right\} \quad (3c)$$

The displacement move is a standard Metropolis scheme where ΔU is the difference between the potential energy of the trial particle after and before the move. For insertion, a particle is inserted from an *infinite* surrounding at constant chemical potential, and $U(N+1) - U(N)$ is the interaction energy of the inserted particle with the other particles and the adsorbent field. For deletion, a particle is chosen at random and removed into the infinite surroundings at constant chemical potential, and the interaction energy of the deleted particle with the other particles is $U(N) - U(N-1)$.

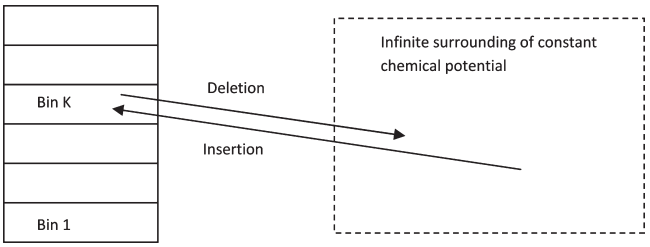

Figure 1. Division of the adsorption space above the surface into bins.

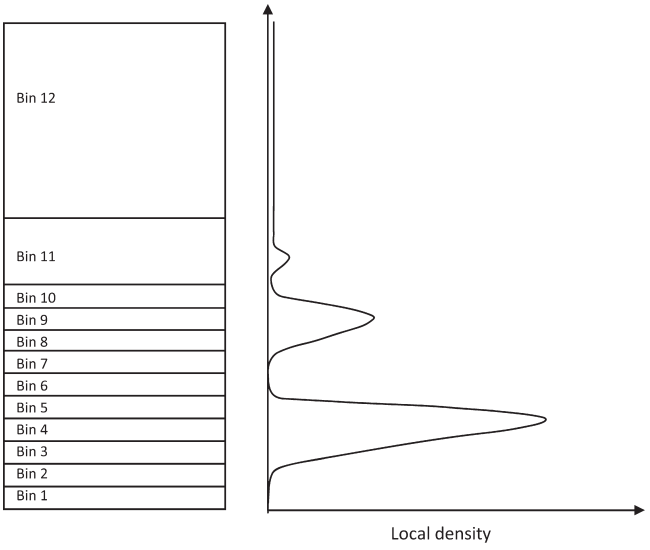

Figure 2. Distribution of bins and their sizes.

In eq 3, N is the number of particles in the *whole* simulation box and takes no account of local density. In the proposed Multibin GCMC, we divide the adsorption space into bins as shown in Figure 1. In the first adsorbed layer, the bin size may be as small as a fraction of the size of a molecule because of the rapid change in density in the first layer; further away from the wall, the density distribution is smoother, and the bin width can be much larger, usually covering the whole gas space outside the adsorbate. The distribution of particles in each bin is taken as being uniform in the directions parallel to the surface for the purpose of choosing bin numbers. The choice of bins for a typical example of adsorption on a surface is shown in Figure 2 for the monolayer region.

Since every bin in the system is exposed to the same chemical potential, each bin itself is a grand canonical ensemble. This means that we can apply the usual GCMC moves. The algorithm for the new scheme is as follows:

1. For each cycle in the *Mu*-GCMC, we do the following M times, where M is the number of bins. First, we choose a bin at random (say bin K) such that all bins are selected with equal probability. We perform insertion and displacement moves in sequence with equal probability. For an insertion

trial, we insert a particle from the infinite surroundings to a random position in bin K. After this move, whether it is successful or not, we perform a displacement move in the same bin. Next we perform a deletion trial (or an insertion trial if the first choice was a deletion to ensure that microscopic reversibility is satisfied). For deletion a particle is selected at random and removed to the infinite surroundings. After this trial, whether it is successful or not, we again perform a displacement. The probability of accepting an insertion or deletion is given by eq 3b or 3c, respectively, with the volume V replaced by V_K and the number of particles N replaced by N_K, i.e.

$$p = \min\left\{1, \frac{V_K}{\Lambda^3(N_K + 1)} \exp\left[\frac{\mu - U(N_K + 1) + U(N_K)}{kT}\right]\right\} \quad (4a)$$

$$p = \min\left\{1, \frac{\Lambda^3 N_K}{V_K} \exp\left[-\frac{\mu + U(N_K - 1) - U(N_K)}{kT}\right]\right\} \quad (4b)$$

Here $[U(N_K + 1) - U(N_K)]$ is the interaction energy of the newly inserted particle in bin K with existing particles of all bins and with the adsorbent field, and $[U(N_K) - U(N_K - 1)]$ is the interaction energy of the randomly selected particle with all the remaining particles and with the adsorbent field.

For a displacement move, we select a particle at random in bin K and move it to another position in the *same bin* and carry out translation and rotation simultaneously if the particle is not spherical. The probability of acceptance is given by the Metropolis equation (eq 3a). The initial maximum displacement length vector, Δ_{max}, is set to be half of the bin length in each direction and adjusted to give an acceptance ratio of 0.2 in that bin as suggested by Mountain and Thirumalai.[12] The acceptance ratio is bin-dependent. There will be no violation of the microscopic reversibility: if particles are displaced within the same bin, they are subject to the same maximum displacement length. If the particle is attempted to be displaced into the adjacent bins, we reject that move. The reason for rejection is that if we allow the particle to cross the boundary we encounter a problem of different maximum displacement lengths in different bins because in the course of the simulation that particle could be displaced back into the bin where it came from (if we allow it to cross the border), but this time it is subject to a different maximum displacement length, violating the microscopic reversibility.

2. The process is repeated for many cycles until equilibrium is reached. The sampling stage is performed in the same way as the equilibration stage, but Δ_{max} is fixed at the value found at the end of the equilibration stage.

Mu-GCMC, as well as reaching equilibrium faster, offers at least two advantages over conventional GCMC.

(a) The maximum displacement length is optimized for each bin being smaller in dense bins and larger in rarefied bins.

(b) The insertion or deletion in each bin is accepted with a probability based on the local density of that bin, rather than the average density of the whole simulation box. This means that when trial insertion is attempted in a bin of low density the probability of acceptance should be greater than in a dense bin because this probability is inversely proportional to the local density (see eq 4a).

2.3.2. Multibin Canonical Monte Carlo (Mu-CMC). In the Multibin Canonical simulation, the simulation box is again divided into bins in the same way as for *Mu*-GCMC (see Figure 2). The volume of the simulation box and the total number of particles are now constant; however, the bin is not a canonical ensemble because the number of particles in each bin fluctuates in the simulation. Let us assume that at final equilibrium the chemical potential of the box is μ (which can be obtained for example by the Widom trial insertion of a test particle). We argue that during the course of the simulation each bin is regarded as a *pseudo* grand canonical with constant volume V_K, constant chemical potential μ, and constant temperature and will show that we do not need to know exactly what this chemical potential is to perform the simulation. Since the number in any given bin is fluctuating, the number in other bins must also change to maintain the total number constant. With this constraint, we perform the simulation by randomly selecting *a pair of bins* such that exchange of particles between these two bins is allowed.

1. The following algorithm summarizes the *Mu*-CMC procedure. For each cycle in the *Mu*-CMC scheme, we do the following C times, where $C = M!/2!/(M - 2)!$ is the number of combinations of two bins selected out of a total of M bins. We select two bins K and L ($K \neq L$) at random. We next select a particle at random in bin K and move it to a random position in bin L, followed by displacements of a randomly selected particle in both bins, irrespective of whether the move is successful or not. Next we select a particle in bin L to move it to a random position in bin K to satisfy the microscopic reversibility. This is then followed by displacements of a randomly selected particle in each bin. This completes the sequence for the pair (K, L). This sequence is made for a randomly selected pair of two bins, no matter how many particles are in any bin. If the number of moves were to be made proportional to the number of particles, this would bias the dense bins in favor of the rarefied bins. Details of these moves are given below.
   a. The move of a particle at random in bin K to bin L may be regarded as a sequence of two steps: the first is deletion of a randomly selected particle in bin K to the surroundings at constant chemical potential, and the second is insertion of a particle from the surroundings to a random position in bin L (see Figure 3). The probability of accepting this move is the product of

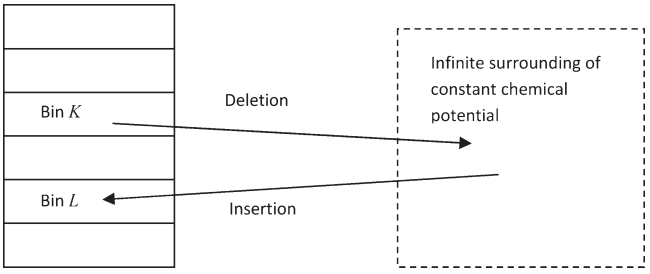

Figure 3. Moving a particle from bin K to bin L is viewed as a deletion of a randomly selected particle in bin K to the surroundings at constant chemical potential and an insertion of a particle from the surroundings into bin L at a random position.

two individual probabilities

$$p = \min\left\{1, \frac{\Lambda^3 N_K}{V_K} \exp\{-[\mu + U(N_K - 1) - U(N_K)]/kT\}\right\} \quad (5a)$$

$$p = \min\left\{1, \frac{V_L}{\Lambda^3(N_L + 1)} \exp\{[\mu - U(N_L + 1) + U(N_L)]/kT\}\right\} \quad (5b)$$

The result of the product of these two probabilities is

$$p = \min\left\langle 1, \frac{(N_K/V_K)}{(N_L + 1)/V_L} \exp\left\{-\frac{[U(N_L + 1) - U(N_L)] - [U(N_K) - U(N_K - 1)]}{kT}\right\}\right\rangle \quad (5c)$$

It is seen that the chemical potential μ disappears from this combined probability as should be expected. Moving a particle from bin K to bin L should not be regarded as a displacement of a particle from bin K to bin L because the process involves moving the particle from an environment of one density to one with a different density. This difference in local density should be reflected in the probability, as can be seen in eq 5c. The difference $[U(N_L + 1) - U(N_L)]$ is the interaction energy of the newly inserted particle at a random position in the bin L with all other particles (including those in other bins) and with the adsorbent, and the energy difference $[U(N_K) - U(N_K - 1)]$ is the energy change for the randomly selected particle in bin K to be removed to the surroundings.

If the displacement move, following the trial insertion/deletion moves, puts the selected particle outside a bin, we reject that move. A displacement trial is accepted with the probability given in eq 3a, and the maximum displacement step length is adjusted to achieve an acceptance ratio of 0.2.

b. The next process in the sequence is to do the opposite to what we just described in part (a). We choose a particle in bin L and move it to bin K. This is to ensure the microscopic reversibility. It is worthwhile to note that the particle that we removed (if successfully) from bin K to bin L in the first process is not necessarily the same particle that we attempt to move from bin L to bin K. For this second process, the probability of acceptance is also given in eq 5c with the subscripts K and L interchanged. Displacement moves are also carried out in the two bins, whether the attempted move is successful or not, and the maximum displacement step length is adjusted to satisfy the acceptance ratio of 0.2.

The advantages of using *Mu*-CMC are:

a. The maximum displacement length is optimized for each bin. Dense bins will be shorter and rarefied bins longer.

b. Insertion or deletion in each bin depends on the density of that bin, rather than the average density of the whole simulation box. This means that when an insertion is attempted in a bin of low density the acceptance probability will be greater than for a dense bin.

The number of successful insertions, N_I^{ins}, and the number of successful deletions, N_I^{del}, and the difference between these two numbers can be followed as a function of cycle number. At equilibrium, since there is microscopic reversibility in every bin, this difference must approach zero, suggesting that this might be used as a criterion for termination of the equilibration stage.

2.4. Choice of Bin Size. The choice of bin size depends on the conditions under consideration (see Figure 2). Essentially we choose it in a manner that particles in the same bin behave roughly the same in an energetic sense. In the bulk gas bin, the density is low and approximately uniform, and over the course of the simulation the ensemble average may only be a fraction of unity. When this bin is selected and there are no particles in the bin, the displacement move will not be counted as an attempted move in the calculation of the acceptance ratio. Furthermore, the acceptance ratio is not calculated until we have attempted at least 10 displacement moves; otherwise, the acceptance ratio is always set at unity. For other bins in which the number of particles is finite, we calculate the acceptance ratio and adjust the maximum displacement length at the end of every 100 cycle, and then the number of attempted displacement moves and the number of successful displacement moves are reset to zero.

2.5. Output from Canonical Ensemble. The MC simulation carried out in a canonical ensemble has a constant number of particles and constant temperature. When the system is divided into bins, the number of particles in each bin fluctuates, and it is possible to determine the variation in number in each bin as a function of the total number in the simulation box. To present the result in a form which is useful to experimentalists, we need to obtain a relationship between the excess density and the pressure (which is the excess isotherm). The excess density is defined as follows

$$\Gamma = \frac{N - \rho_G V}{A} \quad (6)$$

where N is the number of particles in the box; V is the accessible volume of the box; and ρ_G is the bulk gas density. To obtain the excess isotherm, we need to calculate the bulk gas density and the pressure. These can be found from the last bin (bin M say), which is essentially the bulk gas. The bulk gas density is

$$\rho_G = \frac{\langle N_M \rangle}{V_M} \quad (7)$$

We can obtain this by using the pressure virial in the last bin or the ideal gas equation of state if the gas phase is sufficiently rarefied.

To calculate the *differential* heat of adsorption, which is defined as the change of the energy of the adsorbed phase per unit change in excess number, we use the following equation

$$q_{diff} = kT - \frac{\partial\{\langle U \rangle - \langle U_G \rangle\}}{\partial\{N - N_G\}} \quad (8)$$

where $\langle\ \rangle$ is the ensemble average; N_G is the hypothetical number of particles occupying the accessible volume at the same density as the bulk gas; U is the energy of the system; U_G is the energy of

the bulk gas which is obtained as

$$\langle U_G \rangle = \frac{V}{V_M} \langle U_M \rangle \tag{9}$$

Here V_M is the volume of the bulk gas bin, and U_M is the energy of that bin.

2.6. Output from the GCMC. In the GCMC simulations, the excess density and the bulk gas phase density can be obtained in the same way as for the canonical ensemble. The latter, however, can also be obtained from an equation of state, if it is available. For 1C-LJ fluids, the equation of state of Johnson et al. is suitable.[18]

The isosteric heat of adsorption (energy released per unit increment number of molecule added to the adsorbed phase at the expense of a molecule in the gas phase) can be obtained directly from the simulation.[19]

$$q_{st} = \frac{\langle N_G \rangle kT}{f(N_G, N_G)} - \frac{f(U,N) - f(U_G, N_G)}{f(N,N) - f(N_G, N_G)} \tag{10}$$

where U is the potential energy between adsorbate molecules plus that between the adsorbate molecule and the solid substrate, and $f(X,Y)$ is the fluctuation variable which is defined as $f(X,Y) = \langle XY \rangle - \langle X \rangle \langle Y \rangle$.

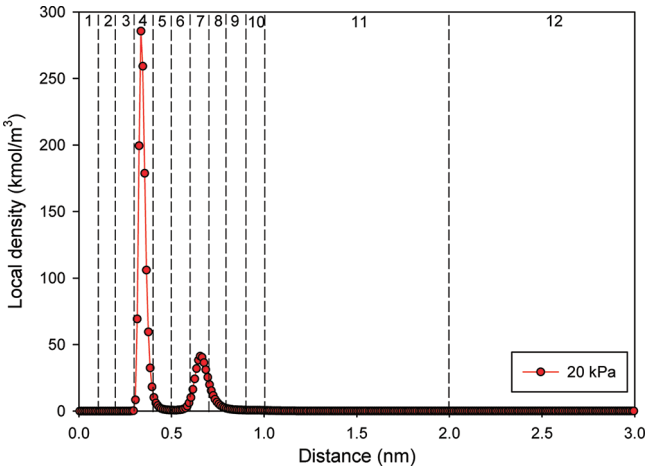

Figure 4. Local density distribution of argon adsorption on a graphite surface at 87.3 K and 20 kPa.

3. RESULTS AND DISCUSSION

3.1. Adsorption of Argon on a Graphite Surface at 87.3 K. To illustrate the new schemes for Monte Carlo simulation in nonuniform systems, we have carried out (*Mu*-GCMC and *Mu*-CMC) simulations for Ar on a graphite surface at 87.3 K. The simulated adsorption isotherm (surface excess versus pressure) and the isosteric heat versus loading are compared with those obtained from the conventional GCMC and CMC.

3.1.1. Mu-GCMC. The graphite surface is placed in the *xy* plane at $z = 0$ in a box with dimensions $10 \times 10 \times 3$ nm in the *x,y,z* directions. The box is divided into 12 bins in the *z*-direction, with the first 10 bins close to the graphite surface having an equal thickness of 0.1 nm and the last two bins having a thickness of 1 nm (Figure 4). The local density distribution at 20 kPa is shown in this figure, and the first 10 bins are chosen to cover the adsorbed layer, which consists of two molecular layers.

The simulated isotherm is shown in Figure 5a as a solid line with red circle symbols. Also plotted in the same figure are the results from a conventional GCMC simulation, shown as a dashed line. The isosteric heats obtained from the two schemes are shown in Figure 5b. It is seen that the results are in excellent agreement, and both describe the experimental data well.[20] For the results presented in this study, the standard deviation has been calculated by determining the ensemble averages from the sets of cycles in the sampling stage and calculating the standard deviation from those averages, and we found that the standard deviation is smaller than the size of the symbols used in all plots.

So what are the advantages of the new scheme *Mu*-GCMC when the conventional scheme can do the task equally well? In Figure 6 we show the plot of the maximum displacement length in the directions parallel to the surface (scaled against the initial displacement length, which is chosen as half of the box length) versus loading in each bin for the *Mu*-GCMC scheme compared with that from the conventional GCMC.

The new scheme shows the change of the maximum displacement length (Δ_{max}) with distance from the surface. It is small for dense bins but is very large for rarefied bins, while for the conventional GCMC the maximum displacement length is the

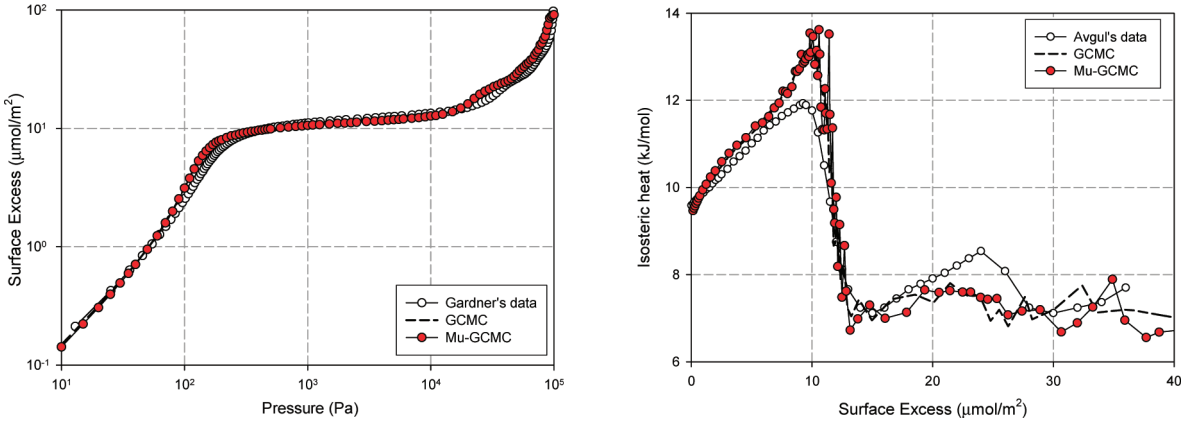

(a) (b)

Figure 5. Simulated isotherm and adsorption heat of argon adsorption on the graphite surface at 87.3 K obtained from GCMC and *Mu*-GCMC and their comparison with the experimental data (unfilled symbols).

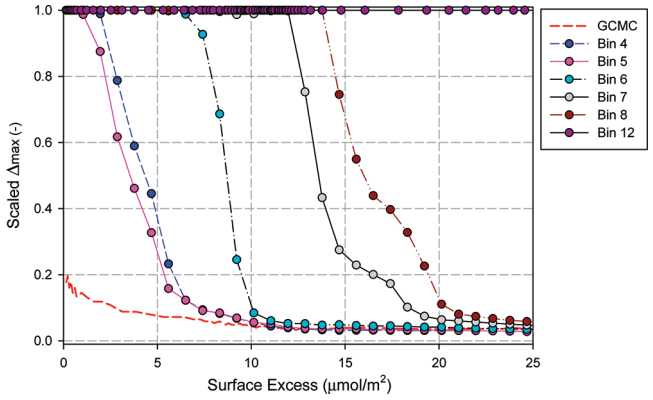

Figure 6. Normalized maximum displacement length versus loading in each bin for the *Mu*-GCMC and that obtained from the conventional GCMC.

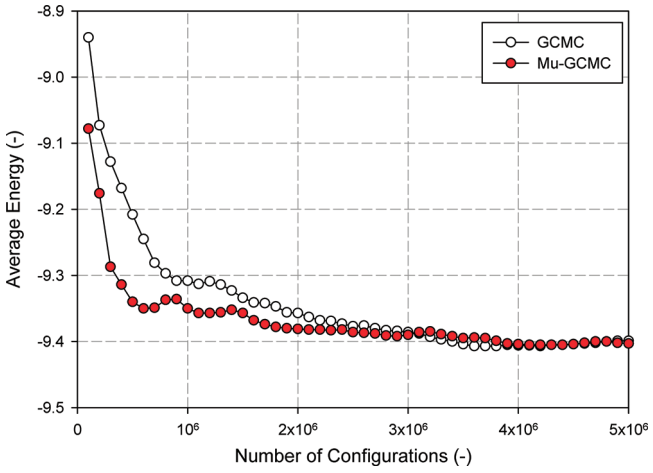

Figure 7. Variation of average particle energy with the number of configurations for argon adsorption on a graphite surface at 87.3 K and 100 Pa. At these conditions, the surface is 40% covered with argon particles.

same for the whole simulation box. Its value is determined mainly by the dense adsorbed layer. We note the following features:

(1) Δ_{max} of the conventional GCMC remains low at all loadings, and it decreases from 0.2 as the loading (pressure) is increased since it is governed by the dense adsorbed phase and is therefore used for all regions including the rarefied regions far away from the surface.

(2) Δ_{max} of each bin in the *Mu*-GCMC also changes with loading, and it remains unity (i.e., half of the box length) when the local loading is low. In bins where the loading is high, Δ_{max} decreases and is asymptotic to the value for conventional GCMC. This means that the new scheme allows particles to be displaced further when the state is rarefied, which means that equilibrium is achieved more rapidly.

To show the advantages of *Mu*-GCMC, we show in Figure 7 the variation in the average particle energy with the number of configurations, which is obtained as the statistical average of the whole system in the equilibration stage. Compared to the conventional GCMC, the *Mu*-GCMC relaxes the system to equilibrium faster. Moreover, not only a smaller number of cycles

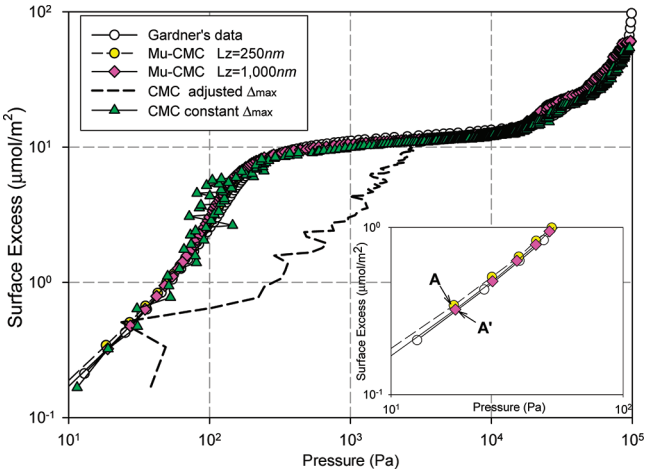

Figure 8. Simulated isotherm of argon adsorption on the graphite surface at 87.3 K obtained from CMC and *Mu*-CMC. The experimental data are shown as unfilled circle symbols.

is required for the new scheme *Mu*-GCMC to reach equilibrium but also the CPU time required by *Mu*-GCMC is much less than that of the conventional GCMC under the same conditions. Take the case shown in Figure 7 as an example, in which there are around 186 particles in the simulation box: the CPU time for the conventional GCMC is 3 times longer than the new scheme *Mu*-GCMC. The efficiency of the *Mu*-GCMC remains true when the simulation system has more particles; for example, at 1000 Pa the number of particles is 640, and the CPU time required by the conventional GCMC is twice as long as *Mu*-GCMC.

3.1.2. Mu-CMC. Unlike the case of grand canonical ensemble, the box size for a canonical (N,V,T) ensemble has to be chosen large enough that the region far away from the surface can be treated as a bulk gas phase uninfluenced by the adsorbed phase. Another reason why this region has to be large is to ensure that there is a sufficient number of particles to be able to estimate the gas density and pressure reliably. This differs from GCMC where there is no interface between the adsorbed phase and the external gas phase. The CMC or the *Mu*-CMC is a better choice if one is interested in the properties of the regions near the interface separating the two phases, and furthermore the canonical system models reality better because in a volumetric adsorption apparatus the adsorption process is canonical (constant total N) rather than grand canonical. Another advantage is that by including the bulk gas we can estimate the gas density and pressure, and this is useful for adsorbates whose equation of state is not known.

For the canonical ensemble, we choose a box size of 10 nm in the x- and y-directions and 250 nm in the z-direction, compared to the box dimensions of 10 × 10 × 3 nm used for the *Mu*-GCMC and GCMC simulations. The bins are selected as shown in Figure 4.

The results from the *Mu*-CMC simulations are shown in Figure 8 as yellow circle symbols and agree well with the experimental data except at very low pressures which is a consequence of the very low average number of particles (much less than unity) in the gas bin which reduces the reliability of the gas density and pressure estimation. At point A for example (see the inset of Figure 8), the statistical average number of particles in the gas bin is 0.19. To have a better estimate of the gas density and pressure, we can choose a larger gas bin to achieve better statistics. Although this means that the simulation box is longer in

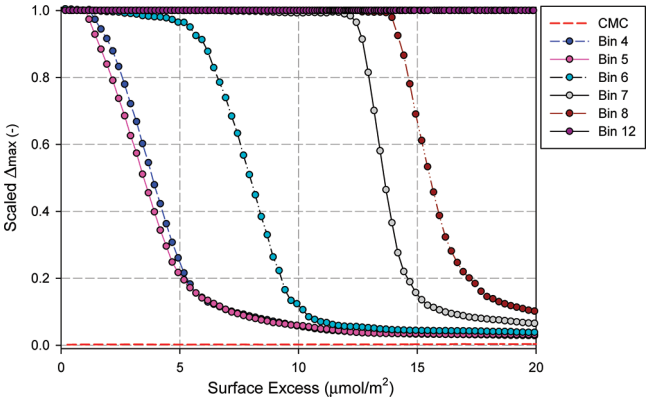

Figure 9. Normalized maximum displacement length versus loading in each bin for the *Mu*-CMC and that obtained from the conventional CMC.

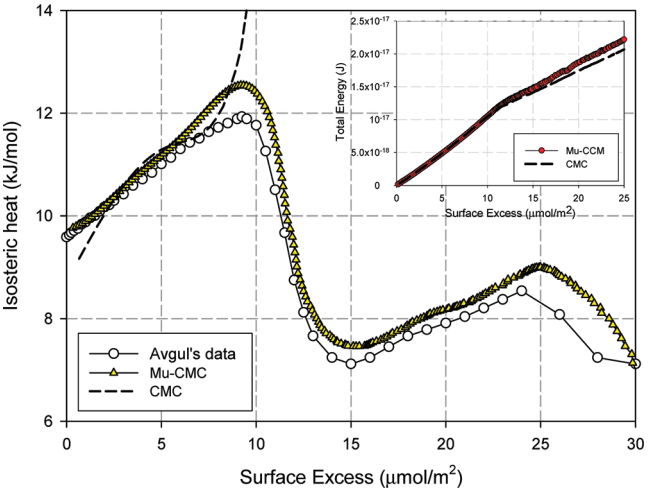

Figure 10. Simulated differential heat of argon adsorption on the graphite surface at 87.3 K obtained from CMC and *Mu*-CMC. The experimental data[20] are also shown for comparison.

the *z*-direction, this does not make the simulation any longer to run than in the smaller box because the gas bin is treated as one bin, no matter how big the simulation box is. We increased the height of the simulation box from 250 to 1000 nm, leaving the first 11 bins the same size as before. The results for this new simulation are shown in Figure 8 as the diamond symbols and solid line. The average number of particles at point A for the larger box is now 0.87, which improves the estimate of the gas density and the agreement between simulation and experimental (see point A′).

To show the potential of the new *Mu*-CMC scheme, we performed a conventional CMC simulation using the box size of $10 \times 10 \times 250$ nm and used the same portion of the simulation box as the bulk gas bin in the *Mu*-CMC simulations to calculate the gas-phase density and pressure. We carried out the CMC in two different ways: (1) in the first approach we adjusted the maximum displacement length (Δ_{max}) such that the acceptance ratio is about 0.2 in the equilibration stage and then kept the value obtained at the end of the equilibration stage for the sampling stage, and (2) we kept the maximum displacement length as half of the simulation box length over the whole course of the simulation. The results obtained from these two different approaches are shown in Figure 8 as the dashed line and triangle symbols, respectively. It is clear that in the conventional CMC it is critical to keep Δ_{max} constant as half of the box length throughout the course of the simulation for the system to reach equilibrium; on the other hand, using the acceptance ratio to adjust Δ_{max} fails to reach equilibrium because Δ_{max} is determined by the dense region of the adsorbed phase and is therefore quite small, and this makes it difficult for the particles in the rarefied regions to sample the space sufficiently to reach equilibrium. In Figure 9 we show a plot of Δ_{max} versus surface excess. As noted previously for *Mu*-GCMC, the Δ_{max} is small for the whole loading range, but in contrast, in *Mu*-CMC, it is small in the dense bins and large in rarefied bins.

3.1.3. Heat of Adsorption. Differential heats (eq 8) obtained from the conventional CMC and *Mu*-CMC are shown in Figure 10 as the dashed line and triangle symbols, respectively. These curves have been smoothed using a smoothing algorithm.[21] The *Mu*-CMC results agree fairly well with the experimental data, but the conventional CMC results fail to describe the data beyond the monolayer region. The reason is that, as we have discussed earlier, conventional CMC requires much longer cycles for the system to reach equilibrium. We also show here the variation of the total energy of the system versus surface excess as an inset in Figure 10; it is clear that the results from conventional CMC are not stable enough for the evaluation of differential heat based on eq 8. Since the results of isotherm and heat from the new scheme *Mu*-CMC are more stable, we only present the results from *Mu*-CMC simulations in what follows.

3.2. Adsorption of Argon on a Graphite Surface at 55 K. In this system, there is a 2D transition in the first layer. The dimensions and number of bins and their sizes were the same as used previously. The isotherm obtained by *Mu*-GCMC is shown in Figure 11a as the filled circles and solid line, and the results from the conventional GCMC are plotted in the same figure. It is seen that the simulations agree qualitatively with the experimental data,[22] and both correctly predict the 2D transition in the monolayer and the second layer. Deviations are observed at the third and higher layers, possibly due to better sampling of space by the *Mu*-GCMC method. The comparison between the isosteric heats obtained by GCMC and *Mu*-GCMC is shown in Figure 11b; the agreement is fairly good for the first two layers, but deviation starts to appear at the onset of the third layer. One interesting point from these simulations is that the maximum isosteric heat predicted by *Mu*-GCMC, which is attained at the completion of the first layer, is 16.6 kJ/mol, while the GCMC scheme gives 14.5 kJ/mol. The difference is attributed to the formation of a 2D solid phase in the first layer, which does not occur in the conventional GCMC simulations. To confirm this, we assume that the heat released is equivalent to the energy of inserting one molecule into a completed CP monolayer with 6 nearest neighbors and 12 next nearest neighbors.[23] Given 9.2 kJ/mol due to solid−fluid (SF) interactions, 6 kJ/mol due to first neighbor interactions, 0.62 kJ/mol from next nearest neighbors, 0.09 and 0.02 kJ/mol from third and higher layers, and 0.46 kJ/mol contributed by the vapor phase, we obtain a heat of 16.4 kJ/mol, which is in better agreement with the *Mu*-GCMC results than conventional GCMC. Another feature which is seen in the plot of the isosteric heat versus loading from GCMC simulation is the discontinuity between the loading of 1 and 10 μmol/m^2, which is the region where the first layer

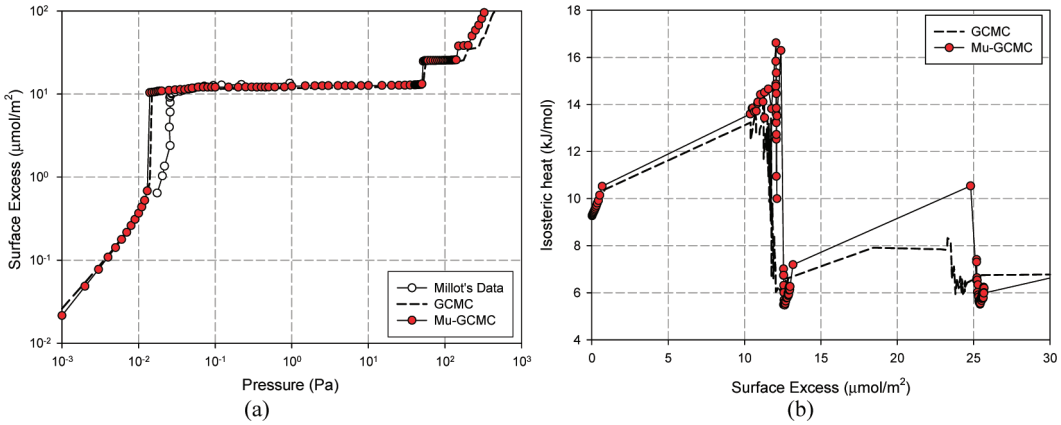

Figure 11. Isotherm and isosteric heat of argon adsorption on the graphite surface at 55 K obtained from GCMC and *Mu*-GCMC. The experimental isotherm is shown with the symbols of open circles.

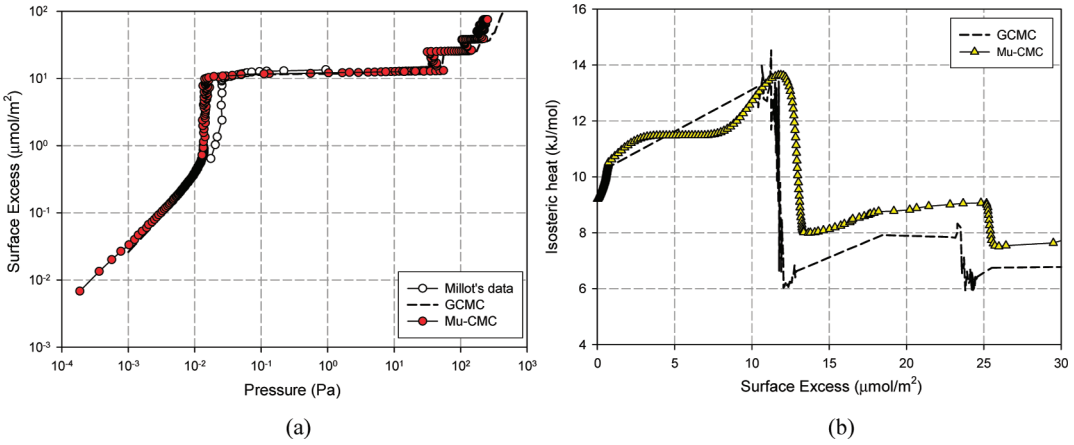

Figure 12. Isotherm and adsorption heat of argon adsorption on the graphite surface at 55 K obtained from *Mu*-CMC, compared with experimental data[22] and the results from GCMC.

2D-transition occurs. The reason is that in the grand canonical ensemble the system is exposed to an infinite surrounding at constant chemical potential. This means that at the onset of the 2D-transition the surroundings will supply enough molecules for the system to reach a new state instantaneously.

To overcome the problem of poor statistics in the gas phase discussed earlier, we enlarged the gas bin by using a box length of 5000 nm in the z-direction and dimensions of 100 nm in the *x*- and *y*-directions. The results are shown as red circle symbols and a solid line in Figure 12a, where we see a reasonably good description of the isotherm compared with the experimental data of Millot[22] and especially of the 2D-transition. Moreover, the *Mu*-CMC allows us to calculate simulation points along the vertical path of the 2D-transition because the number of particles in a canonical ensemble is constant. These points correspond to the constant heat seen in Figure 12b and would be impossible to achieve with the grand canonical ensemble. This is a key feature of the canonical ensemble modeling, and we emphasize again that experiments are performed in a canonical, rather than a grand canonical, system. Indeed, Avgul and Kiselev,[20] in their experimental study of carbon tetrachloride adsorption on graphite, obtained a constant heat of adsorption at temperatures below the triple point because their calorimetric device was canonical. For the 2D-transition in the second and higher layers, sigmoid behavior was observed with the new *Mu*-CMC scheme, as reported by Nguyen et al.[24]

3.3. Adsorption of Argon in Slits at 87.3 K. The new schemes of *Mu*-CMC and *Mu*-GCMC can be readily applied to the study of adsorption in pores, where the gas-phase bin is constructed outside the pore. Here we take argon adsorption in a 2 nm graphitic slit pore at 87.3 K as an example and implement the *Mu*-GCMC simulation. We use 10 bins in the pore and one bulk gas bin external to the pore. The pore dimensions are 5 nm in the *x*- and *y*-directions, and the pore walls are modeled by the Steele 10−4−3 potential separated by a distance of 2 nm between planes through the atom centers of the outer carbon layers. The bin size in the pore is 0.2 nm, and the gas-phase bin is cubic with a linear dimension of 5 nm and with periodic boundary conditions applied in all directions. Conventional GCMC, on the other hand, uses the whole pore as the simulation box. The isotherms obtained by the conventional GCMC and *Mu*-GCMC are shown in Figure 13 as the dashed line and circle symbols, respectively. Again the agreement between the two methods is good in the region before condensation but distinctly different after condensation. This is because in *Mu*-GCMC the volume space is sampled more efficiently; therefore, the system reaches the stable state more readily, while the conventional GCMC moves to metastable states after condensation or evaporation.

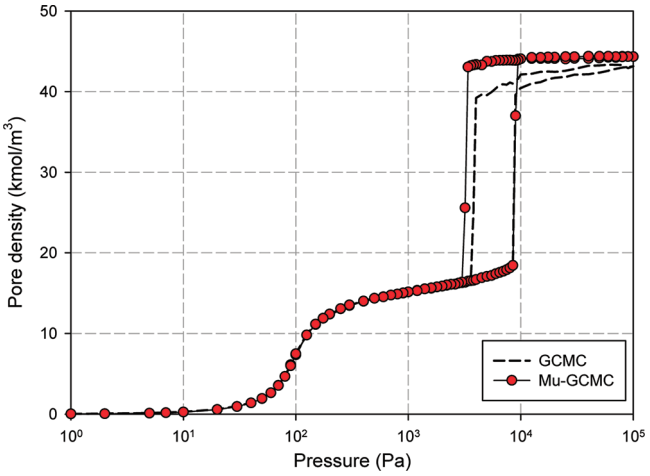

Figure 13. Isotherm for argon adsorption in a 2 nm slit pore at 87.3 K obtained from GCMC and *Mu*-GCMC.

4. CONCLUSIONS

We have presented two new MC schemes *Mu*-GCMC and *Mu*-CMC for simulations of nonuniform systems and illustrate their application with simulations of argon adsorption in the Ar/graphite system. The methods are implemented by dividing the fluid into bins of different sizes that are roughly inversely proportional to the local density. MC moves comprise standard displacements within bins and exchanges between randomly selected bins. In this way every region of the fluid is sampled efficiently. We have shown that these new schemes offer several advantages compared to conventional methods. Although GCMC is widely used for the simulation of adsorption, we point out that an experimental volumetric adsorption system is in fact canonical (i.e., the total number of molecules at each adsorption point is constant). The new method for *Mu*-CMC enables efficient simulation of the canonical ensemble and has the added benefit that the adsorptive phase properties can be found at each isotherm point without the need to resort to an equation of state. We show that certain features observed in earlier experimental data are accessible to canonical ensemble simulations but not to GCMC.

AUTHOR INFORMATION

Corresponding Author

*Fax: +61-7-3365-2789. E-mail: d.d.do@uq.edu.au.

ACKNOWLEDGMENT

This project is supported by the Australian Research Council.

REFERENCES

(1) Vishnyakov, A.; Neimark, A. V. Studies of liquid-vapor equilibria, criticality, and spinodal transitions in nanopores by the gauge cell Monte Carlo simulation method. *J. Phys. Chem. B* **2001**, *105* (29), 7009–7020.

(2) Gubbins, K. E. Molecular adsorption in micropores. *Chem. Eng. Prog.* **1990**, *86* (8), 42–44.

(3) Steele, W. Computer simulations of physical adsorption: a historical review. *Appl. Surf. Sci.* **2002**, *196* (1−4), 3–12.

(4) Kowalczyk, P.; Holyst, R.; Tanaka, H.; Kaneko, K. Distribution of Carbon Nanotube Sizes from Adsorption Measurements and Computer Simulation. *J. Phys. Chem. B* **2005**, *109* (30), 14659–14666.

(5) Kanda, H.; Miyahara, M. Sublimation phenomena of Lennard-Jones fluids in slit nanopores. *J. Chem. Phys.* **2007**, *126* (5), 054703/1–054703/4.

(6) Ohba, T.; Kanoh, H.; Kaneko, K. Cluster-growth-induced water adsorption in hydrophobic carbon nanopores. *J. Phys. Chem. B* **2004**, *108* (39), 14964–14969.

(7) Miyahara, M.; Kanda, H.; Yoshioka, T.; Okazaki, M. Modeling Capillary Condensation in Cylindrical Nanopores. A Molecular Dynamics Study. *Langmuir* **2000**, *16* (9), 4293–4299.

(8) Ohba, T.; Kaneko, K. Cluster-associated filling of water molecules in slit-shaped graphitic nanopores. *Mol. Phys.* **2007**, *105* (2−3), 139–145.

(9) Ohba, T.; Kaneko, K. Surface oxygen-dependent water cluster growth in carbon nanospaces with GCMC simulation-aided in situ SAXS. *J. Phys. Chem. C* **2007**, *111* (17), 6207–6214.

(10) Terzyk, A. P.; Furmaniak, S.; Harris, P. J. F.; Gauden, P. A.; Woch, J.; Kowalczyk, P.; Rychlicki, G. How realistic is the pore size distribution calculated from adsorption isotherms if activated carbon is composed of fullerene-like fragments?. *Phys. Chem. Chem. Phys.* **2007**, *9*, 5919–5927.

(11) Ohkubo, T.; Miyawaki, J.; Kaneko, K.; Ryoo, R.; Seaton, N. A. Adsorption Properties of Templated Mesoporous Carbon (CMK-1) for Nitrogen and Supercritical MethaneExperiment and GCMC Simulation. *J. Phys. Chem. B* **2002**, *106* (25), 6523–6528.

(12) Mountain, R. D.; Thirumalai, D. Quantitative measure of efficiency of Monte Carlo simulations. *Phys. A (Amsterdam, Neth.)* **1994**, *210* (3−4), 453–460.

(13) Frenkel, D.; Smit, B. *Understanding Molecular Simulation: From Algorithms to Applications*; San Diego: Academic Press, 1996; Vol. xviii, p 443.

(14) Do, D. D.; Do, H. D.; Fan, C.; Nicholson, D. On the Existence of Negative Excess Isotherms for Argon Adsorption on Graphite Surfaces and in Graphitic Pores under Supercritical Conditions at Pressures up to 10,000 atm. *Langmuir* **2010**, *26* (7), 4796–4806.

(15) Do, D. D.; Do, H. D. Effects of potential models in the vapor−liquid equilibria and adsorption of simple gases on graphitized thermal carbon black. *Fluid Phase Equilib.* **2005**, *236* (1,2), 169–177.

(16) Steele, W. A. The physical interaction of gases with crystalline solids: I. Gas-solid energies and properties of isolated adsorbed atoms. *Surf. Sci.* **1973**, *36* (1), 317–352.

(17) Steele, W. A. *International Encyclopedia of Physical Chemistry and Chemical Physics, Topic 14: The Interaction of Gases with Solid Surfaces*; Pergamon: Elmsford, NY, 1974; Vol. 3, 356 pp.

(18) Johnson, J. K.; Zollweg, J. A.; Gubbins, K. E. The Lennard-Jones equation of state revisited. *Mol. Phys.: Int. J. Interface Chem. Phys.* **1993**, *78* (3), 591–618.

(19) Do, D. D.; Do, H. D.; Nicholson, D. Molecular Simulation of Excess Isotherm and Excess Enthalpy Change in Gas-Phase Adsorption. *J. Phys. Chem. B* **2009**, *113* (4), 1030–1040.

(20) Avgul, N. N.; Kiselev, A. V. Physical adsorption of gases and vapous on graphitized carbon blacks. *Chem. Phys. Carbon* **1970**, *6*, 1–124.

(21) Press, W. H.; Teukolsky, S. A.; Vetterling, W. T.; Flannery, B. P.; Mercalf, M. *Numerical Recipes in Fortran 90. The Art of Parallel Scientific Computing*, 2nd ed.; Numerical Recipes; Cambridge: Cambridge University Press, 1997; Vol. 2, 1486.

(22) Millot, F. Adsorption of the first layer of argon on graphite. *J. Phys. Lett.* **1979**, *40* (1), 9–10.

(23) Nguyen, V. T.; Do, D. D.; Nicholson, D. On the heat of adsorption at layering transitions in adsorption of noble gases and nitrogen on graphite. *J. Phys. Chem. C* **2010**, *114* (50), 22171–22180.

(24) Nguyen, V. T.; Do, D. D.; Nicholson, D. Monte Carlo Simulation of the Gas-Phase Volumetric Adsorption System: Effects of Dosing Volume Size, Incremental Dosing Amount, Pore Shape and Size, and Temperature. *J. Phys. Chem. B* **2011**, *115* (24), 7862–7871.